Thermal and mechanical assessments of the 3D-printed conformal cooling channels: computational analysis and multiobjective optimization

Suping Shen [1,2,a,#], Baris Burak Kanbur [1,2,b,#], Yi Zhou [1,2,c,#], Fei Duan [2,d,*]

[1] *Singapore Centre for 3D Printing, Nanyang Technological University, Singapore, 639798*

[2] *School of Mechanical and Aerospace Engineering, Nanyang Technological University, Singapore, 639798*

[a] spshen@ntu.edu.sg ; [b] bbkanbur@ntu.edu.sg ; [c] yzhou028@e.ntu.edu.sg ; [d] feiduan@ntu.edu.sg

*# S.P. Shen and B.B. Kanbur share the first authorship; * Corresponding author*

Abstract:

Conformal cooling is an additive manufacturing-based solution and it is a rapidly developing method for reducing the cooling time of the plastic injection process. The present study investigates the thermal and mechanical performances of the 3D-printed conformal cooling channels using computational analyses and multiobjective optimization. For a real injection mold product, two different conformal cooling channel profiles, which are circular and elongated, are analyzed individually. Their cooling time, temperature non-uniformity, and pressure drop are assessed. Compared to the traditional channels, the cooling time of designed CCCs is reduced in the range of 30-60%. The cooling and fatigue life performances of the elongated channel are analyzed for different channel pathways and cross-section areas. As for the circular channel, the coolant temperature, volume flow rate, and channel diameter are selected as the parameters within the ranges of 288.0-298.0 K, 1.0-10.0 L/min, and 2.1-2.5 mm, respectively. According to these parameters, the multiobjective optimization study is performed and the best trade-off point is found at the channel diameter of 2.5 mm, coolant temperature of 297 K, and the flow rate of 1 L/min when all the objectives have equal weights in the optimization problem.

Keywords: Conformal cooling, plastic injection, additive manufacturing, computational simulations, thermal analysis, mechanical analysis, multi-objective optimization.

1. Introduction

Plastic injection molding is a cost- and time-efficient way to manufacture plastic parts so that it is a feasible process for fabricating a mass amount of identical plastic parts quickly. The process is simply explained as the injection of the melted plastic into the mold, where it is cooled and solidified into the final part [1]. In the cycle of injection molding, cooling is the most important step which takes up nearly 70-80% of the total cycle time [2] because the efficiency of injection molding relies largely on it. The improvement of cooling techniques can lead to low cooling time (and inherently cycle time) as well as a high product produced rate. The injection molding cooling is based on the cooling channels that are conventional straight channels fabricated via traditional machining tools (e.g. drilling). However, the recent developments in additive manufacturing (AM) or 3D-printing techniques allow engineers to design more complex but more efficient cooling channel solutions, which are known as conformal cooling channels (CCCs), with the flexibility in shape and size [3, 4]. Since the AM-based CCC solutions have more complex geometric pathways, their design processes are not as simple and basic as the traditional channels so that a more powerful design approach is required such as computer-aided engineering (CAE) [5]. The CAE process can be explained via two steps as follows: the first step of this approach is to design the CCC based on the plastic shape by computer-aided design (CAD). After that, the thermal and mechanical performance of different CCC designs (e.g. cooling time, fatigue life) can be numerically evaluated and compared by computational fluid dynamics (CFD) software. Many publications have proven the strength of CAE tools. Shen et al [6] designed a serpentine CCC with different cross-section profiles. Its cooling and mechanical performances under different coolant flow rates and inlet temperatures were simulated by ANSYS and validated by experimental data. The results showed that the cooling time of CCC can be shorted by from 10% to 57.1% compared with the traditional straight channel. Suchana et al [7, 8] developed a numerical model to predict the thermal and mechanical performances of designed CCC in plastic

injection molding. The important design dimensions of CCC were analyzed by the design of experiments. The final design of CCC was 3D printed in Maraging Steel powder by using Truprint 3000 metal 3D printing machine [9]. Park et al [10] proposed a framework that integrates commercial CAD–CAE software by using common scripting. The proposed method could reduce the computing cost of structural optimization. Kanbur et al [11] analyzed the thermal and mechanical performances of conformal cooling cavities supported by lattice structures computationally in the ANSYS environment. It is revealed that the designs could achieve significantly lower cooling time values than the reference straight channel. However, the mechanical properties of the conformal cooling cavities still need further improvement studies. Au et al [12] evaluated the cooling performance of a CCC design in the blow molding process by integrating CAD and CAE tools. The proposed CCC design provided shorter cooling time and smaller part temperature compared with the traditional straight channel. Despite improvements, the design and simulation steps are not enough for real CCC cases. In real applications, the final decision is generally done using the optimization approach. The decision-making procedure is complex and the optimization approach depends on the selected objective functions. Up to now, the optimization studies were carried out according to the analytical-1D models [13] and the CAE models [14, 15] for the single objectives such as warpage thickness, cooling time, thermal stress, etc. To this end, it can be said that the design, simulation, optimization, and decision-making steps of the CCCs are complex; and therefore, a comprehensive approach is required to provide fast, reliable, and affordable solutions in the industry. More details on the comprehensive approach can be found in our recent review study [5].

Although the above-mentioned studies performed remarkable efforts on the analysis of conformal cooling solutions, there is still a lack of research gap to better understand the thermal and mechanical performances of the conformal cooling applications including their final decision-making steps. To deal with the challenges of these comprehensive requirements, this paper proposes an approach that consists of both CAE-based thermal & mechanical simulation and multiobjective optimization. For this purpose, an injected model geometry, which is currently being used in the real industry, is selected and

the design criteria are defined with respect to the operating conditions in the factory and 3D printability. Two CCCs with elongated and circular cross-section profiles are designed to cool a plastic product. Computer-aided engineering (CAE) simulations are performed for investigating and evaluating the thermal and mechanical performance of the elongated and circular CCCs. Different cross-section areas and pathways of elongated CCC are discussed. The elongated CCC is analyzed only with CAE simulations while the circular CCC is used in the multi-objective optimization procedure after carrying out the CAE simulations. The cooling water temperature (CWT), volume flow rate (VFR), and channel diameter (CD) of circular CCC are considered as optimization parameters. According to the operating conditions and design limitations of the circular CCC, the cooling time (CT), temperature non-uniformity (TU), and pressure drop (PD) are defined as the multiple objectives that are aimed to be minimized. The multi-objective optimization study is performed in the MATLAB environment via the genetic algorithm (GA) tool. In this way, a comprehensive approach is defined from the design step to the decision-making step, which is performed via the weighted-sum method, in order to present an efficient methodology for the design engineers, mold engineers, and optimization operators who work in the injection molding processes.

2. Computational Thermal Model

Figure 1 shows the entire injection molding process that consists of the main coolant inlet and outlet, auxiliary cooling channels, plastic part & runner, and conformal cooling channel. The CCC in the figure is designed as an alternative to the currently-in-operation reference straight channel that belongs to our industrial partner. The entire process is used as in the computational thermal model. The forepart of the CCC is inside the plastic product. The flow pathway and the cross-section of elongated CCC are presented in Figure 2(a) and (b). Two pathways are designed for elongated CCCs in this study and their dimensions are presented in Table 1. For each pathway, the length (g) and width (h) of the cross-section shown in Figure 2(b) are given in Table 2. The h only has two values, 1.5 and 2.0 mm. For each h, there are 6 values of g, from 2.5mm to 5.0mm with an interval of 0.5mm. Figure 2 (c) gives the flow path and the cross-section profile of circular CCCs.

The channel diameter (CD) of the circular channel is defined between 2.1 and 2.5 mm with 0.1mm interval.

During the injection molding cooling process, the temperature of plastic decreases, and the coolant undergoes temperature increase and pressure drop. The plastic material is polybutylene terephthalate (PBT), the mold material is steel, and the coolant is water. The thermophysical properties of the steel and PBT are assumed independent of temperature variations and they can be seen in Table 3. The mass, momentum, and energy equations of three-dimensional, unsteady flow and heat transfer are given as:

（1） mass continuity equation

$$\nabla \cdot \vec{\boldsymbol{u}} = 0 \tag{1}$$

（2） momentum equation

$$\rho \frac{\partial \vec{\boldsymbol{u}}}{\partial t} + \rho \vec{\boldsymbol{u}} \cdot \nabla \vec{\boldsymbol{u}} = -\nabla p + \mu \nabla^2 \vec{\boldsymbol{u}} \tag{2}$$

（3） energy equation

$$\rho C_p \left(\frac{\partial T}{\partial t} + \vec{\boldsymbol{u}} \cdot \nabla \boldsymbol{T} \right) + \nabla \cdot (-k \nabla T) = 0 \tag{3}$$

where $\vec{\boldsymbol{u}}$ is velocity vector, ρ is the density, t is time, p is the pressure, μ is the dynamic viscosity of water, C_p is the heat capacity, T is the temperature, k is the thermal conductivity. In the steel molding domain, there is only a heat conduction mechanism. The corresponding energy equation in this domain is:

$$\rho C_p \frac{\partial T}{\partial t} + \nabla \cdot (-k \nabla T) = 0 \tag{4}$$

To solve the governing equations, a finite element software, ANSYS, Fluent 19.2, is employed in this study. Since the *Re* number of water flow is large, the standard $k - \varepsilon$ turbulence model is selected whilst the pressure-velocity coupling method is defined with the SIMPLEC algorithm. The second-order upwind scheme is used to discretize the governing equations. Figure 3 presents the

time step independent check results. It is seen that further reduction doesn't remarkably affect the plastic temperature when the time step reaches to 0.1s by gradually reducing. Thus the time step of 0.1s is chosen as the time step of the simulation study. To assess the thermal performance, we choose the objectives of cooling time (CT), temperature non-uniformity (TU), and coolant pressure drop (PD). The cooling time of injection molding is the time when the plastic temperature reaches the ejection temperature. The plastic injection and ejection temperatures are defined as 543K (270℃) and 323K (50℃), respectively. The temperature non-uniformity is the surface integration standard deviation of the plastic temperature, which can be withdrawn from the ANSYS CFD database. Small temperature non-uniformity indicates the temperature distribution of plastic product is uniform, which is good for its quality.

Figure 4 projects the sectional view of the tetrahedral mesh generated on the geometry. The mesh is refined near the CCC area. For all elongated CCCs, the volume flow rate (VFR) and coolant temperature (CWT) are fixed at 7L/min and 294K, respectively. As for circular CCC, the range of VFR and CWT is 1-10L/min and 288-298K, respectively. The reason behind different operating values (or ranges) between the elongated and circular CCCs is the optimization purpose. For the elongated CCC, we only perform computational mechanical and thermal simulations whilst the circular CCC has an additional optimization step. Thus, it is worth noting that we have finalized the CAE simulations and focused on the optimization of the circular CCC since our previous efforts already convinced us to define the most convenient operating parameters of the circular CCC design. However, the CAE simulations of the elongated CCC are still on-going so that the optimization step is still not ready. For the optimization of the circular CCC, the total case number is 125. The plastic walls are in coupled boundary condition for all cases. The boundary condition of the straight cooling channel walls is the convective thermal condition. To maintain consistency with the real industrial experiment, the temperature of liquid coolant inside these straight channels is 323K. The initial temperature of the plastic product is 543K (270℃), and the ejection temperature is 323K (50℃).

Figure 5 shows the plastic temperature results of the mesh independency study. The mesh cell number increases from 0.4 million to 2 million gradually. The decreasing curve of the plastic temperature with the flow time under different mesh numbers are given in Figure 5. When the mesh number reaches 1.2 million and above (up to 2 million), the decreasing curve doesn't change so that we can clearly say that the mesh independency is achieved and the mesh cell number of 1.2 million is selected for the computational thermal simulations in this paper.

To verify the computational model, we compared the model conditions with the experimental results. For this purpose, we applied the same computational boundary conditions to the reference straight cooling channel, which is already in operation by our industrial partner, and we compare the results of computational thermal simulation and the experimental study. The comparison is based on the cooling time and the temperature of the plastic product after 10 s and the comparisons can be seen in Table 4. According to the obtained results, it can be said that the relative errors are low and acceptable for verification.

3. Computational Mechanical Model

Besides the thermal model, mechanical performances are also critical for the 3D-printed injection molds. Thus, we conducted computational mechanical simulations in the ANSYS Mechanical environment. The mechanical simulation model can be seen in Figure 6(a). The proposed product improvement is for the mold part (see conformal cooling channels Figure 1) and other parts are the same as the currently operated plastic injection unit. Hence, we only focus on the mold part during the mechanical simulations; and hereby, we could save computational time and cost. Figure 6(b) presents the boundary conditions of mechanical computation. The red surfaces in Figure 6(b) contact with the melt polymer directly, which is cooled down to form the aimed plastic product. So a pressure boundary condition with a value of 50MPa is set for these surfaces. As for the yellow regions B and C, the displacement boundary condition is set as shown in Figure 6(b). Region B has 0.15mm displacement along Z-axis and it is free in the X and Y-axis. Region C has 0mm

displacement along the X and Y-axis and it is free in Z-axis. The automatic mesh is used for the meshing. Unlike the thermal model, there is no need for transient mechanical simulations since the steady mechanical analysis already validates its accuracy with respect to the collected experimental fatigue life results by our industrial partner.

4. Multi-objective Optimization Model

By using the verified computational thermal model, the parametric thermal analysis is done for different CWT, VFR, and CD parameters in the range of 288- 298 K, 1-10 L/min, and 2.1-2.5 mm, respectively. For each CD value, 25 different CFD results are obtained according to different CWT and VFR values. The CD parameters are evaluated with 0.1 mm intervals; thus, the CFD study generated 125 different results. The collected results are created as a 3D matrix in the MATLAB environment; then, the matrix is defined as the initial population of the GA for the multi-objective optimization tool. The multi-objective optimization study generates the Pareto frontier plot that projects the best trade-off points according to the GA solution. The multi-objective optimization is defined in Eq. 5,

$$MOF = \min[f(CT)] \& \min[F(TU)] \& \min[F(PD)] \quad (5)$$
$$288\text{K} \leq CWT \leq 298\text{K}$$
$$1\ L/min \leq VFR \leq 10 L/min$$
$$2.1mm \leq CD \leq 2.5mm$$

The selection of the best trade-off points depends on the decision maker's criteria so that the selection depends on the defined weights for each objective function. This approach is known as the weighted-sum model that is defined in Eq. 6,

$$MS = a \cdot f^*(TU) + b \cdot f^*(CT) + c \cdot f^*(PD) \quad (6)$$

where *a, b,* and *c* are the weights of objective functions and the summation of the weights (a+b+c) equal to 1. Besides, the normalized function, f^*, is defined with the utopia and pseudo-nadir points of the objective functions as shown in Eq. 7,

$$f^* = [f(x) - f^U(x)]/[f^{PN}(x) - f^U(x)] \quad (7)$$

where $f^U(x)$ and $f^{PN}(x)$ denote the utopia and pseudo-nadir values, respectively. According to Eqs. 6 and 7, the best trade-off point can be selected with respect to different weights.

5. Results and Discussion

5.1 Elongated CCCs Results

Figure 7 shows an illustrative example of the temperature gradients on the plastic product cooled down by the designed elongated channel (Pathway 1, g=4.5mm, h=2mm). Similar to the illustrative example, the temperature values are collected for all cases to calculate the cooling time and temperature non-uniformity. After collecting the transient thermal data, the cooling time (CT) trends are presented in Figure 8. It is found that Pathway 2 has lower results for different cross-section dimensions because it is closer to the plastic walls compared to Pathway 1. For both two pathways, when h equals 2.0mm, CT is also lower because of the large cross-section area. Also, the cooling time decreases by increasing of g value. When all cases are considered, the CT ranges between 2.8 and 4.9 as shown in Figure 8(a). Compared to the CT of traditional straight cooling channel, which is nearly 7s according to the experimental results of our industrial partner, the proposed elongated CCCs can shorten the cooling time from 30% to 60%. Figure 8(b) shows the trends of the temperature non-uniformity (TU). It is found that CT and TU have opposite trends. Figure 8(c) is the pressure drop (PD) of designed elongated CCCs with different dimensions. PD decreases by increasing of cross-section area. Also, Pathway 2 has slightly higher PD than that of Pathway 1, which is most probably because of faster temperature changes in the Pathway 2 channel since it is closer to the plastic wall. The foregoing thermal performance trends state that there is no common increasing or decreasing trend among the problem objectives. Thus, the obtained results push us to carry out further decision-making strategies (e.g. multi-objective optimization) for the elongated CCC.

Figures 9 denotes the Von Mises stress contour of the mold with elongated CCC (Pathway 1, g=2.5mm, h=1.5mm). All the resulting stresses of different channels are lower than the acceptable upper limit of yield strength of the mold material. Thus, when using the designed serpentine channels, the structure of the mold is stable. The maximum stress of the elongated CCC is at the turning corner of the mold as indicated in Figure 9. This simply means the further mechanical performance improvements can be considered independent of channels and directly focus on the turning corners, which can be efficiently handled by the 3D-printing process. Figures 10(a) and 10(b) are the fatigue life results of Pathways 1 and 2, respectively. Since Pathway 2 has a closer distance between the channel wall and the plastic walls, its fatigue life is lower than that of Pathway 1. Nevertheless, in any case, both pathways present satisfying mechanical performance. The fatigue life decreases with the increasing of the cross-section dimension g, which is understandable.

5.2 Circular CCCs Results

Like the elongated CCC, the transient computational thermal analysis calculates the cooling time, temperature non-uniformity, and pressure drop for each circular CCC design with a total number of 125 CFD simulations. The CT of the circular CCCs in the defined parametric range is shown in Fig. 11(a). The results infer that the CT increases by rising of the CWT. From 288 K to 298 K, the average increment rate of CT is found nearly 11.8%. The VFR values have also significant impacts on the CT trends and it is seen that the increase of VFR from 1 to 10 L/min achieve critical decrement in CT, but it is worth mentioning that the increment of VFR also results in the increment of pump operation cost. From the minimum VFR to the maximum, the CT decreases by averagely 32.65% and the decrement rate show a very slight difference when the different CD values are compared. On the other hand, it is seen that the CT drops by nearly 4.67%. The comparative assessment amongst the impacts of parameters, the impact of CD has the minimum while the VFR and CWT have crucial impacts. Apart from the CT trends, the TU trends are projected in Figure 11(b). The minimization of TU is the desired point for the process of the mold. The TU trends decrease by increasing of the CWT from 288K to 298 K, but the decrement

trend is not the same for each VFR, and it drops when the VFR increases. For example, when the data of CD=2.5 mm is investigated, the decrement of TU from 288K to 298 K is nearly 31.67% at the VFR of 1 L/min; however, the decrement of TU is calculated as 24.58% at the VFR of 10 L/min. The reason behind this outcome is not only related to the impact of CWT but also related to the VFR trends. From minimum VFR to the maximum one, the TU increases dramatically by 23.14%. Moreover, it is seen that the TU increases by 3.49% from the CD of 2.1 mm to 2.5 mm. Similar to the outcome of CT trends, the TU trends also deduce that the impact of CD is very low compared to the CWT and VFR. In addition to the TU and CT trends, the pressure drop (PD) trends are plotted in Figure 11(c).

The PD trends are simply based on the VFR and CD parameters since the CWT does not affect the pressure drop. The PD has higher values at the lowest CD and the highest VFR values. The difference between the highest and lowest VFR is significant; namely, the PD at the VFR of 10 L/min is 82.3 times higher than the PD at the VFR of 1 L/min. Even though the CD parameters also affect the PD trends, the impact of CD is very small compared to the impact of VFR on the PD trends. When the PD data is compared between the CD of 2.1 and 2.5 mm, the CD of 2.1 mm has nearly 1.37 times higher PD values than the CD of 2.5 mm. It is also worth to mention that the PD trends are important to define the pump work well for the real-scale industrial process. Higher PD simply means higher pump work that results in higher energy consumption and relevant energy (operation) costs. Therefore, the PD has a direct link to the operation cost and its minimization is a crucial factor.

In the mechanical analysis, the boundary conditions of the designed circular CCCs are the same as the elongated CCCs. Thus, we can say that the channel profile does not have a crucial impact on the mechanical strength. Also, the fatigue life trends of the circular CCCs are found similar to the traditional straight cooling channel. Therefore, the mechanical performance of the designed circular CCC-based mold geometry seems satisfying and the fatigue life cycle is not

considered as one of the multiple objectives in the optimization study and the following decision-making step.

5.3 Multi-objective Optimization Results

After analyzing the CT, TU, and PD trends, the results are defined in 3D matrices in the MATLAB environment and used as the input of the GA algorithm in the multi-objective optimization tool. The optimization procedure is built according to Eq. (5), and the Pareto frontier is obtained with 18 different optimal solutions as shown in Figure 12.

It is observed that the optimal points are distributed in a wide region and the selection of the best tradeoff point is strictly up to the decision maker's criteria. According to the obtained points in the Pareto frontier, the weighted sum (WS) approach is performed after normalizing the objective functions according to their utopia and pseudo-nadir points (see Eq. (6) and (7)). To see the impact of different weights for each objective function, various values of a, b, and c (see Eq. (6)) are considered and the results are presented in Table 5. The table states that the CWT and VFR are the dominant parameters for determining the best trade-off point at different function weights and this outcome is in a good agreement with the results of the CFD analysis that deduce that the impact of CD is very small compared to the CWT and VFR. The last column of Table 5 denotes the optimal point numbers in the Pareto frontier and those points are already shown in Figure 12. It is seen that the CWT and VFR have opposite trends; and therefore, the selection of the best trade-off point depends on their weightings. To this end, it can be said that the impact of these two parameters must be analyzed and considered very well; and then, the decision-making must be completed. There are pros and cons to these two objectives. When the minimum CWT is aimed, the extra chiller power can be required to cool down the CWT from the supplied temperature to the design temperature, and this process increases the energy consumption of the water cooling system in the factory. According to Table 4, the corresponding VFR value to the minimum CWT is the highest and this also increases the required pump rate that causes extra energy consumption. Moreover, all the

optimal points denote that the CD of 2.5 mm is the optimum value for the diameter and this is a valuable outcome since obtaining a single value of CD means there is a single optimal value for the CD which cannot be changed during the system operation and can only be decided during the mold manufacturing (3D printing) step.

6. Conclusion

A comprehensive approach on the design, analysis, simulation, and optimization of the CCC-based injection molds was proposed by performing the computer-aided engineering tools since the entire process of the CCC-based molds is based on the 3D printing technology and this makes the whole process difficult and complex to solve with the traditional techniques. The computational thermal and mechanical analysis was performed to see the channel performance from the viewpoints of cooling time, temperature non-uniformity, pressure drop, and mechanical performance, which were critical for the industrial process in a real manufacturing operation. The performance of different cross-section area and the pathway of elongated CCCs were compared. According to the system parameters of cooling water temperature (288-298 K), volume flow rate (1-10 L/min), and the channel diameter (2.1-2.5 mm), the performance of circular CCCs were discussed. After that, the multi-objective optimization was performed in the MATLAB environment with genetic algorithm. The CFD analyses showed that the channel diameter had a very small impact on the defined objectives. The volume flow rate and the cooling water temperature were the dominant factors according to the Pareto-frontier plot of the multi-objective optimization procedure. The best trade-off point depended on the weights of the objective functions. In light of foregoing, the future studies can focus on the wider understanding of the optimization problem by considering the cost of consumed electricity (related to the cooling of circulated water and the pump operation) and the alternative CCC pathway. Also, the presented elongated CCC results motivated for initiating the multi-objective optimization studies by considering various multiple objectives. To this end, after their optimization studies, the optimum geometries can be sent to the lab-scale printing process to see the impact of operating parameters on the printing quality, which will help

us to better understand the relation between the operating parameters of CAE, printing quality, and further understanding of the life cycle assessments of the 3D-printed injection molding tools.

Acknowledgement

The authors would like to sincerely thank the support of the Singapore Centre for 3D Printing (SC3DP) and the School of Mechanical and Aerospace Engineering for this original research work.

Nomenclature

AM:	Additive Manufacturing	f^U:	Utopia value of the objective function
a-f:	Dimensions of the elongated pathways	f^{PN}:	Pseudo-nadir value of the objective function
CCC:	Conformal Cooling Channels	*FL:*	Fatigue Life (Cycles)
CAD:	Computer-Aided Design	*GA:*	Genetic Algorithm
CAE:	Computer-Aided Engineering	*g and h*	Length and width of elongated channel cross-section
CD:	Channel Diameter of circular channel (mm)	*MOF:*	Multi-objective Function
CFD:	Computational Fluid Dynamics	*PD:*	Pressure Drop
CT:	Cooling Time (s)	*TU:*	Temperature Non-uniformity (K)
CWT:	Cooling water temperature (K)	*VFR：*	Volume Flow Rate (L/min)
f:*	Normalized function	*WS:*	Weighted-Sum

References

[1] Z. Shayfull, S. Sharif, A.M. Zain, M.F. Ghazali, and R.M. Saad, Potential of Conformal Cooling Channels in Rapid Heat Cycle Molding: A Review. Adv Polym Tech, 2014, 33, p 21381–21381.

[2] M.S. Shinde, K.M. Ashtankar, A.M. Kuthe, S.W. Dahake, and M.B. Mawale, Direct Rapid Manufacturing of Molds with Conformal Cooling Channels. Rapid Prototyp J, 2018, 24(2), p1347–1364.

[3] W.E. Frazier, Metal Additive Manufacturing: A Review. J Mater Eng Perform, 2014, 23, p 1917-1928.

[4] Y. Zhang, L. Wu, X. Guo, et al, Additive Manufacturing of Metallic Materials: A Review. J Mater Eng Perform, 2018, 27, p 1-13.

[5] B.B. Kanbur, S.P. Shen, and F. Duan, Design and Optimization of Conformal Cooling Channels for Injection Molding: A Review, Int J Adv Manuf Tech, 2020, 106, p 3253-3271.

[6] S.P. Shen, B.B. Kanbur, Y. Zhou and F. Duan, Thermal and Mechanical Analysis for Conformal Cooling Channel in Plastic Injection Molding, Mater Today Proc, 2020, 28, p 396-401.

[7] A.J. Suchana, T. Wu, Y. Zhang, et al, Thermo-mechanical Design Optimization of Conformal Cooling Channels Using Design of Experiments Approach. Proc Manuf, 2017, 10, p 898-911.

[8] A.J. Suchana, H. El-Mounayri, Optimal Conformal Cooling Channels in 3D Printed Dies for Plastic Injection Molding, Proc Manuf, 2016, 6, p 888-900.

[9] A.J. Suchana, T. Wu, Y. Zhang, et al, Thermo-fluid Topology Optimization and Experimental Study of Conformal Cooling Channels for 3D Printed Plastic Injection Molds, Proc Manuf, 2019, 34, p 631-639.

[10] Park, H.S., and Dang, X.P., 2010, Structural Optimization based on CAD-CAE Integration and Metamodeling Techniques, Comput. Aided Des, 42, pp.889–902.

[11] B.B. Kanbur, S.P. Shen, Y. Zhou and F. Duan, Thermal and Mechanical Simulations of the Lattice Structures in the Conformal Cooling Cavities for 3D Printed Injection Molds, Mater. Today Proc, 2020, 28, p 379-383.

[12] K.M. Au, K.M. Yu, Conformal cooling channel design and CAE simulation for rapid blow mold, Int J Adv Manuf Tech, 2013, 66, p 311-324.

[13] X. P. Dang and H. S. Park. Design of U-Shape Milled Groove Conformal Cooling Channels for Plastic Injection Mold, Int J Precis Eng Manuf, 2011, 12, p 73–84.

[14] H.S. Park and X.P. Dang. Structural optimization based on CAD-CAE integration and metamodeling techniques, Comput. Aided Des, Vol. 42, No. 10, pp. 889–902, 2010.

[15] H.S. Park and X.P. Dang. Optimization of conformal cooling channels with array of baffles for plastic injection mold. Int J Precis Eng Man 2010, 11, 879–890

Figures:

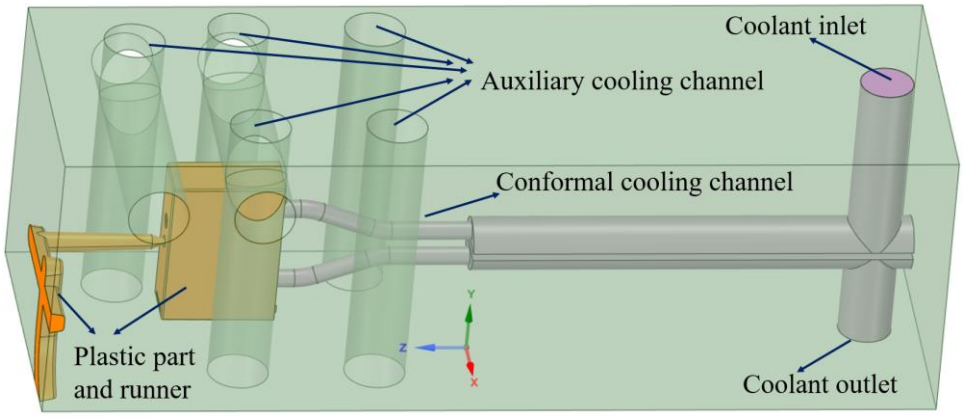

Figure 1. Computational geometric model of the entire plastic injection process.

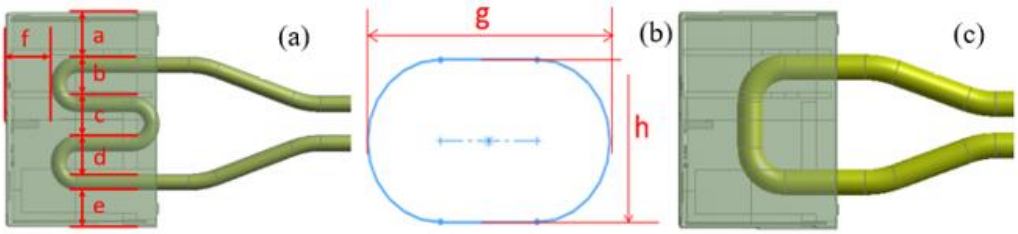

Figure 2. The designed CCC; (a) flow path and (b) cross-section profile of elongated CCCs; (c) flow path of circular CCCs.

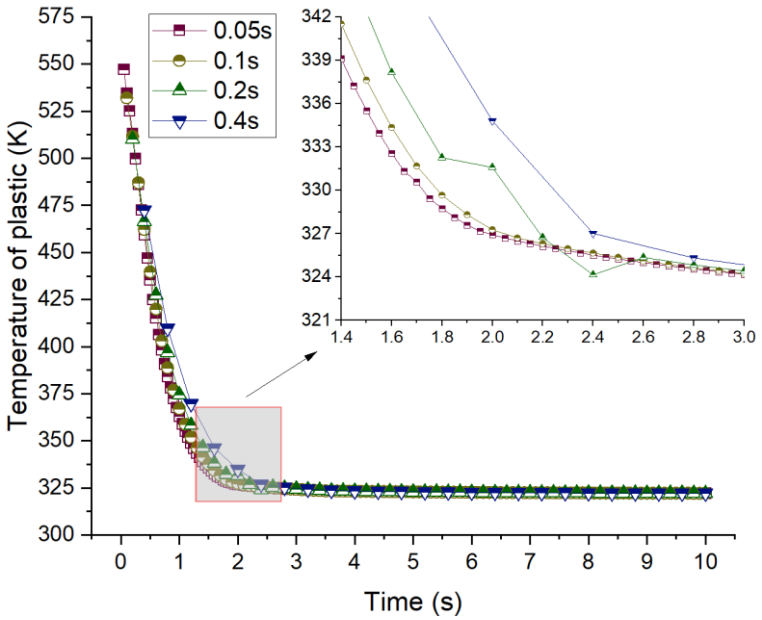

Figure 3. Time step independent check results

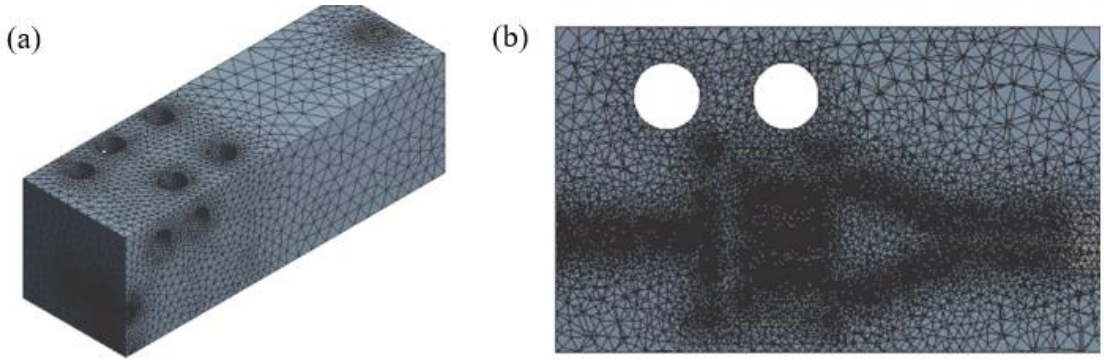

Figure 4. Mesh generation: (a) 3D view, (b) refined CCC area in sectional view

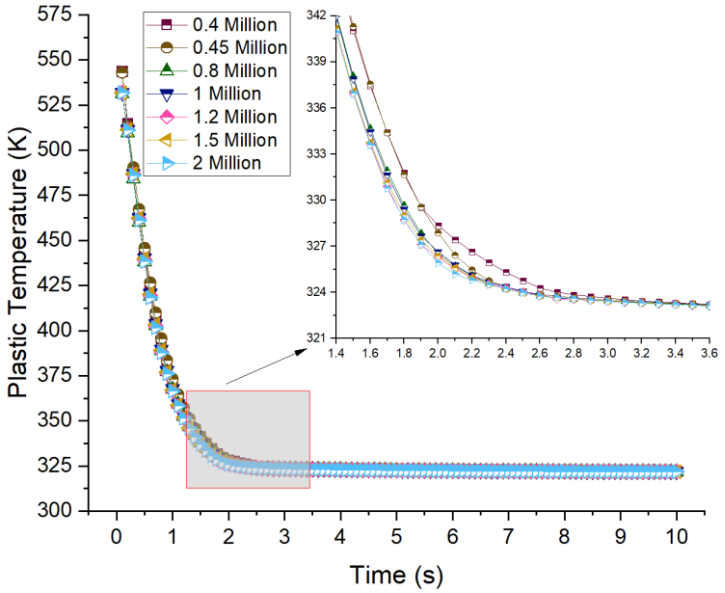

Figure 5. Mesh independent check: Plastic temperature decreasing with flow time

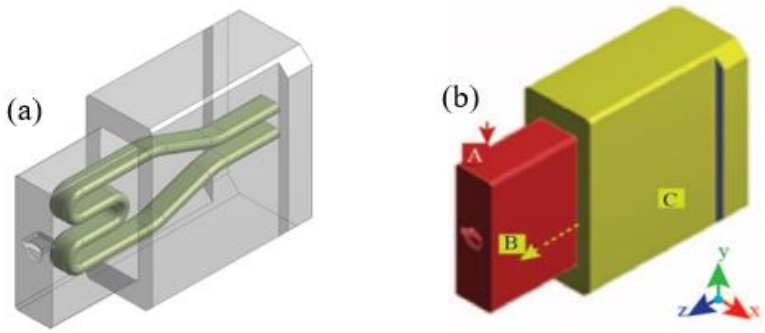

Figure 6. Mechanical computation model (a) Mold part with elongated CCC; (b) Boundary condition of mechanical computation: red region A is pressure boundary condition, yellow region B and C is displacement boundary condition.

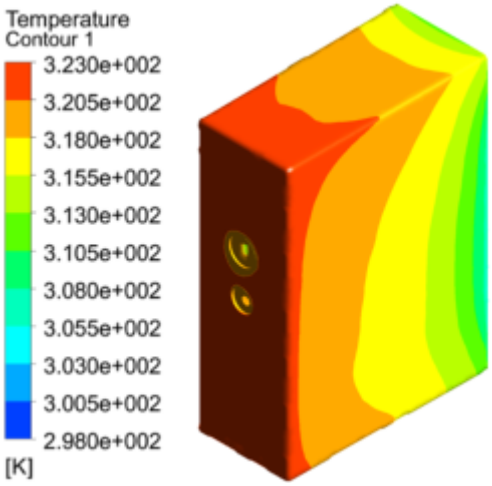

Figure 7. Temperature contour of plastic cooled by the elongated CCCs: Pathway 1, g=4.5mm, h=2mm (Unit: Kelvin)

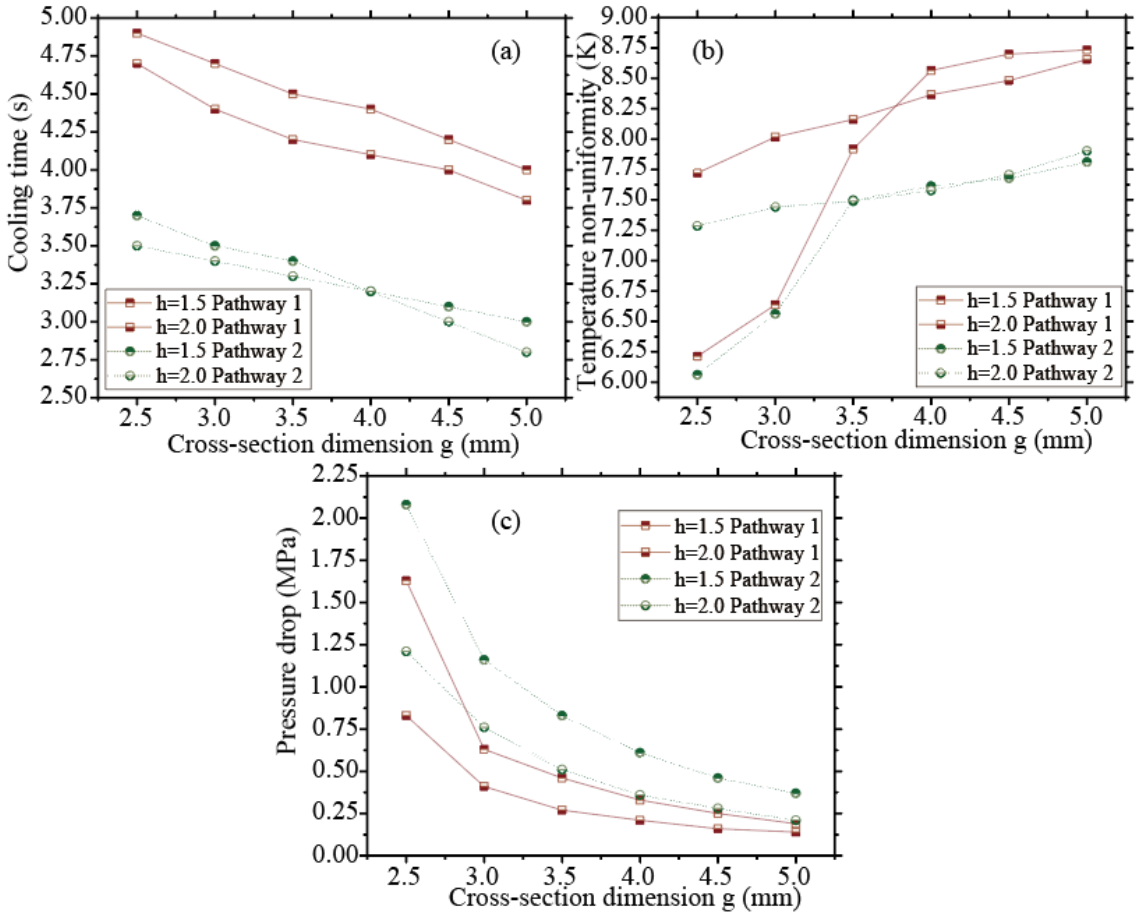

Figure 8. Thermal simulation results of plastic product cooled by elongated CCCs: (a) cooling time (s), (b) temperature non-uniformity (K), (c) pressure drop (MPa).

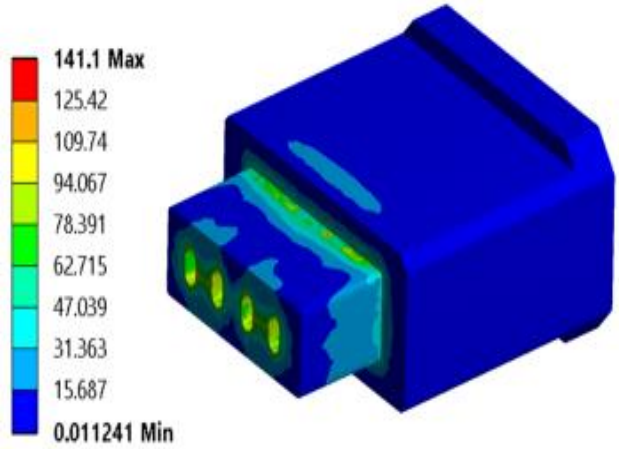

Figure 9. Von Mises stress of mold part with the elongated CCC: Pathway 1, g=2.5mm, h=1.5mm (unit: MPa)

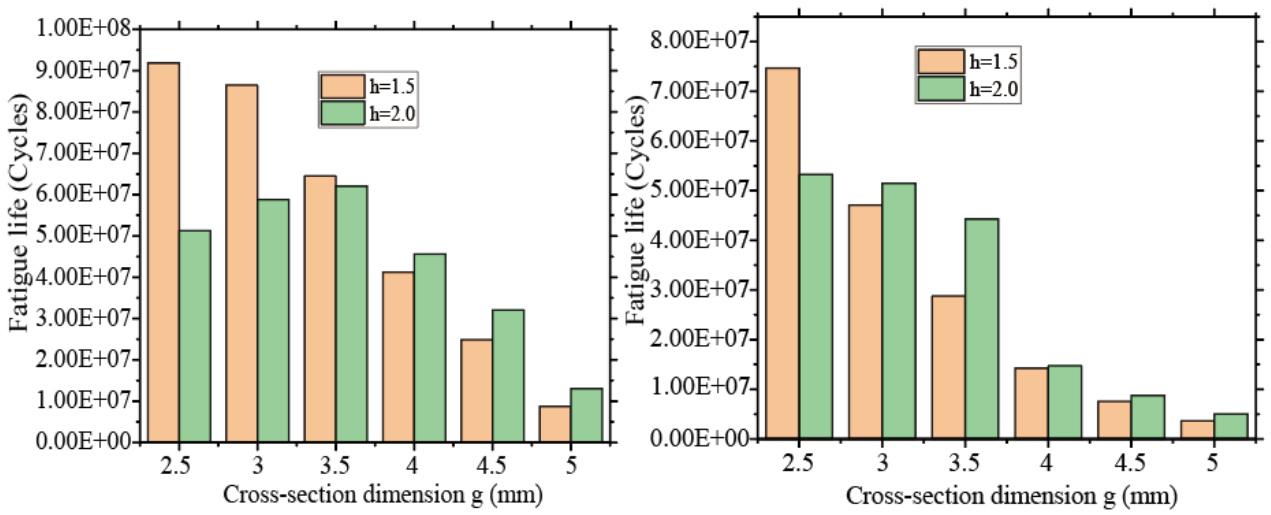

Figure 10. Fatigue life results of mold part with the elongated CCCs: (a) pathway 1 and (b) pathway 2 (unit: cycles)

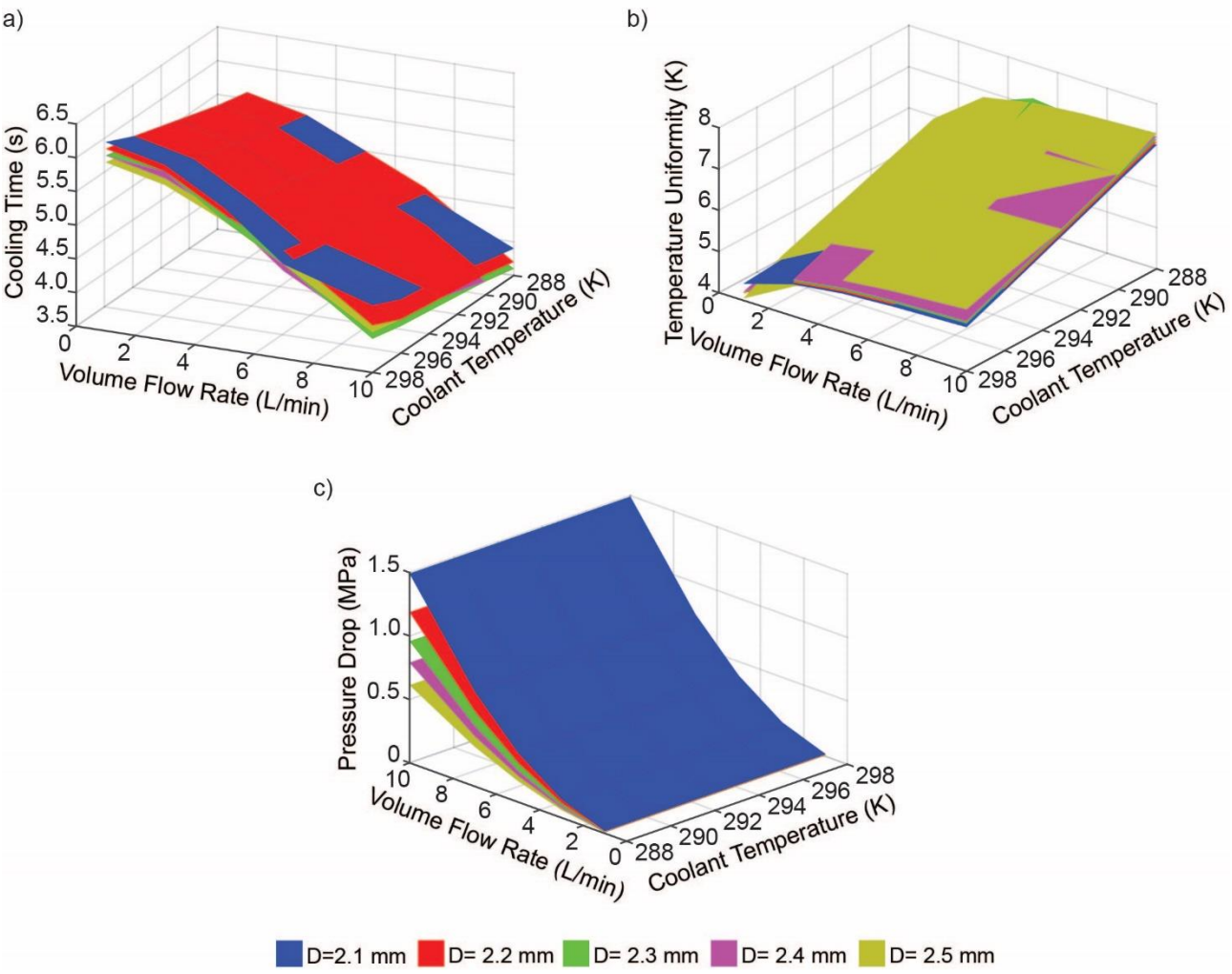

Figure 11. Thermal results of plastic product cooled by circular channel: (a) cooling time (s), (b) temperature non-uniformity (K) and (c) pressure drop (MPa).

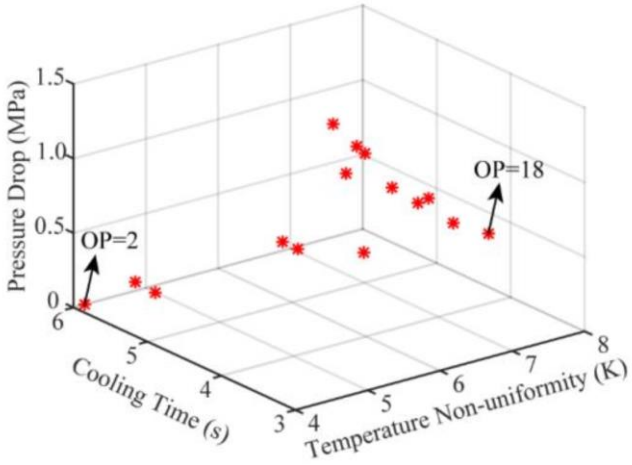

Figure 12. Pareto frontier of the multi-objective optimization procedure

Tables:

Table 1. Dimensions of two flow pathways of elongated CCCs (Unit: mm)

Pathway	a	b	c	d	e	f
1	3.5	3.5	3.5	3.5	3.5	3.5
2	2.4	4.4	4.8	4.4	2.4	2.5

Table 2. Dimensions of the cross-section of elongated CCCs (Unit: mm)

g	2.5, 3, 3.5, 4, 4.5, 5	2.5, 3, 3.5, 4, 4.5, 5
h	1.5	2.0

Table 3. Thermophysical properties of the plastic and steel [6].

Material/Property	Polybutylene terephthalate (PBT)	Steel
Density (kg/m^3)	1396	8030
Specific heat (J/kgK)	1363	502.48
Conductivity (W/mK)	0.2883	16.27

Table 4. Verification of computational thermal model with experiments [6].

	Cooling time (s)	Plastic temperature after 10s cooling (K)
Experimental data	7	338
Numerical results	6.5	333
Relative error (%)	7.14%	1.48%

Table 5. Pareto optimal solutions with respect to various function weights

a/b/c (Eq. 6)	CWT (K)	VFR (L/min)	CD (mm)	Optimal point No.
0.1/0.2/0.7	297.68	1.01	2.50	2
0.1/0.4/0.5	288.00	9.98	2.50	18
0.1/0.6/0.3	288.00	9.98	2.50	18
0.1/0.8/0.1	288.00	9.98	2.50	18
0.2/0.1/0.7	297.68	1.01	2.50	2
0.33/0.33/0.33	297.68	1.01	2.50	2
0.4/0.5/0.1	297.68	1.01	2.50	2
0.6/0.1/0.3	297.68	1.01	2.50	2
0.8/0.1/0.1	297.68	1.01	2.50	2